STUK - A 156 July 1998

The eighth National Electromagnetics Meeting

August 27, 1998

Extended abstracts

Esko Eloranta, Kari Jokela (eds.)

STUK • SÄTEILYTURVAKESKUS • STRÅLSÄKERHETSCENTRALEN
RADIATION AND NUCLEAR SAFETY AUTHORITY

The conclusions presented in the STUK report series are those of the authors and do not necessarily represent the official position of STUK.

ISBN 951-712-267-5
ISSN 0781-1705

Oy Edita Ab, Helsinki 1998

Available from:
STUK—Radiation and Nuclear Safety Authority
P.O. Box 14, FIN-00881 Helsinki, Finland
phone: +358-9-759881
fax: +358-9-75988500

ELORANTA, Esko, JOKELA, Kari (eds.). The eighth National Electromagnetics Meeting. August 27, 1998. Extended abstracts. STUK-A156. Helsinki 1998. 49 pp.

ISBN 951-712-267-5
ISSN 0781-1705

Keywords electromagnetic fields, electromagnetic waves, electromagnetic radiation, Maxwell's equations, analytical methods, numerical methods, computational science

SUMMARY

The National Electromagnetics Meeting has been arranged annually since 1991 in Finland. The purpose of the meeting is to convene the persons working with problems of electromagnetics and to enhance the interaction between different research groups in different disciplines.

The eighth meeting was held at the Radiation and Nuclear Safety Authority (STUK) August 27, 1998. The meeting is also the national meeting of the URSI (L'Union Radio-Scientifique Internationale) (Commission B: Fields and Waves) and the IEEE MTT/AP/ED Finland Chapter (Institute of Electrical and Electronics Engineers, Inc.).

The report includes the extended abstracts of the presentations given in the National Electromagnetics Meeting at STUK.

ELORANTA, Esko, JOKELA, Kari (toim.). Kahdeksas valtakunnallinen Sähkömagnetiikan seminaari 27.8.1998, laajat tiivistelmät. STUK-A156. Helsinki 1998. 49 s.

ISBN 951-712-267-5
ISSN 0781-1705

Avainsanat sähkömagneettiset kentät, sähkömagneettiset aallot, sähkömagneettinen säteily, Maxwellin yhtälöt, analyyttiset menetelmät, numeeriset menetelmät, laskennallinen tiede

YHTEENVETO

Suomessa on järjestetty vuosittain kansallinen sähkömagnetiikan seminaari vuodesta 1991 alkaen. Seminaarin tarkoituksena on ollut koota yhteen sähkömagnetiikan parissa työskenteleviä henkilöitä eri tieteen ja tutkimuksen aloilta sekä lisätä näin eri alojen välisiä vuorovaikutuksia.

Kahdeksas seminaari pidettiin 27.8.1998 Säteilyturvakeskuksessa. Seminaari on samalla URSI:n (L'Union Radio-Scientifique Internationale) Commission B:n (kentät ja aallot) sekä IEEE MTT/AP/ED Finland Chapterin (Institute of Electrical and Electronics Engineers, Inc.) kansallinen kokous.

Raportti sisältää Säteilyturvakeskuksessa pidettyjen esitelmien laajat tiivistelmät.

PREFACE

The National Electromagnetics Meeting has been arranged since 1991 in Finland. The purpose of the meeting is to convene the persons working with problems of electromagnetics and to enhance the interaction between different research groups in different disciplines.

The eighth meeting was held at the Radiation and Nuclear Safety Authority (STUK) August 27, 1998. The meeting is also the national meeting of the URSI (L'Union Radio-Scientifique Internationale) (Commission B: Fields and Waves) and the IEEE MTT/AP/ED Finland Chapter (Institute of Electrical and Electronics Engineers, Inc.). The meeting was supported by the IEEE.

This report includes the extended abstracts of the presentations given in the meeting at STUK. As editors of the report we would like to thank all the lecturers and participants for their contributions to the meeting. Special thanks are reserved for Professor Jukka Sarvas, the Head of the Rolf Nevanlinna Institute of the University of Helsinki, for his support in arranging this meeting and for the creation of the WWW Home Pages of the National Electromagnetics Meeting (http://www.RNI.Helsinki.FI/Sähkömagnetiikka/). Also the help from the Electromagnetics Laboratory of the Helsinki University of Technology is gratefully acknowledged.

Esko Eloranta

Kari Jokela

CONTENTS

FAST CALCULATION OF GEOMAGNETICALLY INDUCED FIELDS APPLYING THE COMPLEX IMAGE METHOD

Ari Viljanen and Risto Pirjola
Finnish Meteorological Institute, Geophysical Research Division
P.O.B. 503, FIN-00101, Helsinki, Finland

Olaf Amm
Technical University of Braunschweig,
Institute of Geophysics and Meteorology
Mendelssohnstr. 3, D-38106 Braunschweig, Germany

Calculation of the transient electromagnetic field connected with geomagnetic variations requires the ionospheric currents and the earth's conductivity as input data. The currents may be assumed to consist of a thin horizontal sheet at a height of about 110 km. There are also geomagnetic-field-aligned currents which ensure that the total current system has no divergence. If the earth's conductivity is modelled by uniform layers then the electric and magnetic field can be expressed as complicated Fourier integrals over the frequency and two spatial wave numbers. They can generally be evaluated only numerically, which may be very time-consuming even in efficient computers. Different image methods have been developed to overcome this problem by replacing the integrals by simpler, often closed-form, formulas.

In this work we are particularly interested in the auroral region phenomena. Then we can assume that the field-aligned currents are vertical. We also apply layered earth conductivity models. These assumptions make it possible to derive convenient closed-form expressions for the electromagnetic field due to a current system which consists of a straight finite-length horizontal filament and of vertical currents at both ends ("elementary |_|-current"). The complex image method (CIM) for horizontal currents has been presented in previous literature (*Thomson and Weaver*, 1975). "Complex" refers here to the frequency-dependent complex depth of the image current. To be able to utilize the previous CIM results, *Pirjola and Viljanen* (1998) have proved that the current system can be replaced by a purely horizontal current distribution which is equivalent regarding the total (= primary + induced) magnetic field and the

total horizontal electric field at the earth's surface. The latter result is a new one. Numerical calculations demonstrate that CIM is very accurate and several magnitudes faster than the exact conventional approach.

Any horizontally spatially limited ionospheric current system can be constructed of elementary |_| -currents. Each element can have any time dependence, and CIM may be applied after performing the Fourier transform to the frequency domain (in practice FFT). After CIM calculations, the field is obtained by the inverse FFT in the time domain.

The ionospheric current used in this work are mostly based on the models derived by *Amm* (1995). Detailed descriptions are given for some typical ionospheric events occurring during auroral storms: an electrojet, the Harang discontinuity, omega bands, and the westward travelling surge.

One application of CIM is to determine the geoelectric field which drives geomagnetically induced currents (GICs) in power networks. A special interest is paid to the largest GICs, because they may be harmful to the power system (*Kappenman*, 1996). GICs are connected with rapid temporal and spatial variations of ionospheric currents. This requires an accurate description of the ionospheric currents by a grid of a size of 50 km × 50 km, the number of grid points being even some thousand.

Another example of the applicability of CIM is to estimate the source field effect in magnetotelluric (MT) studies. The standard MT methods rely on the plane wave assumption of the inducing field, which is often invalid at high latitudes. The effect of spatially inhomogeneous ionospheric currents on the MT responses can be easily estimated by CIM.

References

Amm, O., 1995: Direct determination of the local ionospheric Hall conductance distribution from two-dimensional electric and magnetic field data: Application of the method using models of typical ionospheric electrodynamic situations. *Journal of Geophysical Research*, **100**, 21473–21488.

Kappenman, J.G., 1996: Geomagnetic Storms and Their Impact on Power Systems. *IEEE Power Engineering Review*, May 1996, 5–8.

Pirjola, R. and A. Viljanen, 1998: Complex Image Method for Calculating Electric and Magnetic Fields Produced by an Auroral Electrojet of a Finite Length. Accepted for publication in *Annales Geophysicae*, 19 p.

Thomson, D. J., and J. T. Weaver, 1975: The Complex Image Approximation for Induction in a Multilayered Earth. *Journal of Geophysical Research*, **80**, 1, 123–129, 1975.

SÄHKÖMAGNETIIKKA 98 SEMINAARI
ELECTROMAGNETICS '98 SEMINAR

Säteilyturvakeskus
Radiation and Nuclear Safety Auth.

Electrostatic images for underwater anisotropic conductive half spaces

Mikko Flykt, Esko Eloranta*, Ismo Lindell
Electromagnetics Laboratory, Helsinki University of Technology
P.O. Box 3000, 02015 HUT
* Radiation and Nuclear Safety Authority
Nuclear Waste and Materials Regulation
P.O. Box 14, FIN-00881 Helsinki, Finland
e-mail: mikko.flykt@hut.fi, esko.eloranta@stuk.fi, ismo.lindell@hut.fi

Abstract – A static image principle makes it possible to derive analytical solutions to some basic geometries for DC fields. The underwater environment is especially difficult both from the theoretical and practical point of view. However, there are increasing demands that also the underwater geological formations should be studied in detail. The traditional image of a point source lies at the mirror point of the original. When anisotropic media is involved, however, the image location can change and the image source may be a continuos, sector-like distribution. In this paper some theoretical considerations are carried out in the case where the lower half space can have a very general anisotropy in terms of electrical conductivity, while the upper half space is assumed isotropic. The reflection potential field is calculated for different values of electrical conductivity.

The case of two conducting half spaces is relevant when we study deep-seated underwater bottom and geological layers beneath it using such electrical systems in which we lower transmitters and receivers in deep water near or within bottom. What is meant by 'deep-seated bottom' is of course relative and it is dependent on the scale of interest. In our model this means that the boundary between water and air can be omitted.

This paper shows an effort to determine the electric potential due to static (or low-frequency) current source in the vicinity of anisotropically conducting half space. The duality principle gives us the possibility to utilise recent results derived for electrostatic permittivity problems. In [1], the well-known image theory for a point charge in front of an isotropic half space, is generalised to an anisotropic half space, where the permittivity tensor characterising the anisotropy is symmetric and positive-definite, i.e., it has three orthogonal eigenvectors and the corresponding eigenvalues are positive. The derivation of the theory resembles Heaviside operational calculus [2] involving pseudodifferential operator manipulations. Although the derivation of the image requires considerable amount of algebraic labour the final result, the image function itself, is compact and readily usable in eg. electric potential calculations.

Consider two conducting half spaces with a plane boundary at $z = 0$, as in the figure (1.a). A point current source $i_0(\mathbf{r}) = I_0\delta(z - z_0)$ is located in an isotropic conducting half space at $z = z_0$, above an anisotropic half space ($z < 0$). Using the image principle, we replace the lower half conductivity with the same, isotropic one, as the upper half is, and compensate the change with an image source. For general anisotropy the image consists of a point source and a surface current distribution over an angular sector, and in [1] it was given in the form

$$i^r(\mathbf{r}) = -I_0\frac{\alpha-1}{\alpha+1}\delta(\mathbf{r}+\mathbf{u}_z z_0) + I_0\frac{2\alpha\beta^2(-(z+z_0))}{\pi\sqrt{\beta^2(z+z_0)^2 - x^2}}\times$$

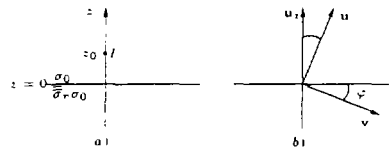

Figure 1: a) geometry of the problem: b) tilted anisotropic medium: it can viewed as rotated $\mathbf{u}_x$, $\mathbf{u}_y$, $\mathbf{u}_z$ axial medium

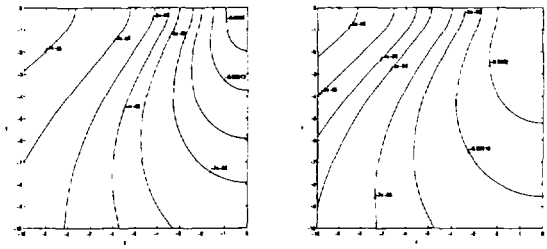

Figure 2: left: reflected potential at $z = 0$ caused by the sector-like image. $\sigma_0 = 3.2$ [S/m], $\sigma_u = 0.1$, $s_v = 0.02$, $s_w = 0.01$, $\varphi = 10°$, due to symmetry the contours can be mirrored with respect to the x and y axes to get the equipotentials for x, y=-10..+10; right: as in left, $\varphi = 65°$

$$\frac{\alpha^2[\beta^2(z+z_0)^2 - x^2] - x^2}{(\alpha^2[\beta^2(z+z_0)^2 - x^2] + x^2)^2}\delta(y)\Theta[\beta^2(z+z_0)^2 - x^2]\Theta[-(z+z_0)] \tag{1}$$

Here, $\alpha^2(1+\beta^2)$ and α^2 are the eigenvalues of a two-dimensional, symmetric and positive-definite dyadic $\overline{\overline{A}}$ which is related to the conductivity dyadic

$$\overline{\overline{A}} = -\det\overline{\overline{\sigma}}_r(\mathbf{u}_z \times \overline{\overline{\sigma}}_r^{-1} \times \mathbf{u}_z) = \alpha^2(1+\beta^2)\mathbf{u}_x\mathbf{u}_x + \alpha^2\mathbf{u}_y\mathbf{u}_y \tag{2}$$

In general, the eigenvectors of σ_r are distinct from those of $\overline{\overline{A}}$. The step functions Θ confine the sector to the lower half space, the apex is at $z = -z_0$.

For a tilted anisotropy (figure (1.b)) we get

$$\alpha = \sqrt{\sigma_w(\sigma_v \sin^2\varphi + \sigma_u \cos^2\varphi)}, \quad \beta = \sqrt{\frac{\sigma_u\sigma_v - \sigma_w\sigma_v \sin^2\varphi - \sigma_w\sigma_u \cos^2\varphi}{\sigma_w\sigma_v \sin^2\varphi + \sigma_w\sigma_u \cos^2\varphi}} \tag{3}$$

and the reflected electric potential in the upper half space is calculated from the integral $\int i^r(\mathbf{r})dV'/(4\pi s_0|\mathbf{r} - \mathbf{r}'|)$ over the image charge, figure 2.

The authors wish to thank Dr. Ari Viljanen for helpful discussions.

References

[1] I. V. Lindell, K. I. Nikoskinen, and A. Viljanen. Electrostatic image method for the anisotropic half-space. IEE Proceedings. Science, Measurement and Technology, 144(4):156–162. 1997.

[2] O. Heaviside. Electromagnetic Theory. Ernest Benn. Ltd, London, 1925. 2nd reprint. Vols. I, II. III.

Electromagnetic Field Computation in Axisymmetric RF Structures with Boundary Integral Equations

Pasi Ylä-Oijala
Rolf Nevanlinna Institute
PO Box 4 (Yliopistonkatu 5), FIN-00014
University of Helsinki, FINLAND
e-mail: Pasi.Yla-Oijala@RNI.Helsinki.FI
tel: +358-9-191 22775 fax: +358-9-191 22779

In this talk we present an accurate time-harmonic field computation algorithm based on the boundary element method (BEM) [1]. Our algorithm is capable of modelling axisymmetric resonators having both electric and magnetic ends, and of modelling segments of coaxial or circular waveguides having possibly ceramic dielectric windows. In waveguides this leads to modelling the standing waves. The computed fields are applied to the analysis of electron multipacting [2], [3] in the superconducting TESLA accelerator cavities and rf power input couplers (see Figure 1). For multipacting we need to consider also traveling and mixed waves. Traveling and mixed waves can be generated by appropriately combining two standing wave solutions. The discussion here is confined to fields in $TM_{0,m,l}$-mode, i.e., the fields are also axisymmetric.

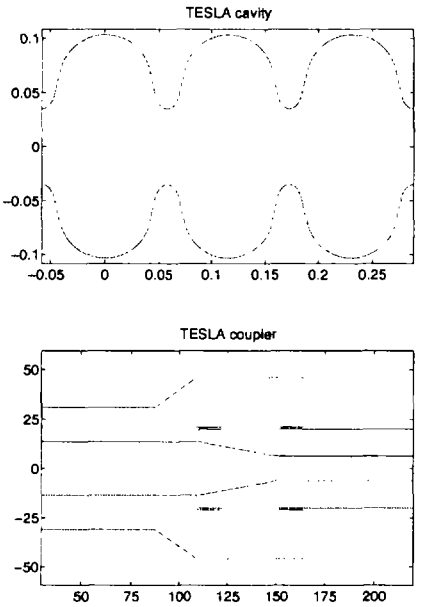

Figure 1: Cross sections of three cells of the TESLA accelerator cavity (dimensions in m) and of the coaxial part of the TESLA input coupler (dimensions in mm). The ceramic window is denoted by shading.

We use a standard boundary integral equation approach based on the Stratton-Chu formulas with the free-space Green's function. The solution of the integral equations is found by

using the Galerkin method with piecewise linear basis functions. This discretization leads to a homogeneous matrix equation, which is solved for a nontrivial solution using the singular value decomposition of a matrix. Furthermore, we have developed accurate integration quadratures and used elliptic integrals to evaluate the singular integral equations numerically.

Due to the field singularities at the junctions of the dielectric and metal surfaces, the BEM turns out to be numerically instable. We can improve the numerical stability by overdetermining the equations on the surfaces of the dielectric window. We illustrate the accuracy of the method in some test cases, where the analytical solutions are available. Furthermore, we study the numerical stability of different integral formulations when the discretization is made denser.

References

[1] P. Ylä-Oijala and E. Somersalo: Computation of Electromagnetic Fields in RF Structures with Boundary Integral Equations, manuscript, (submitted to *Journal of Electromagnetic Waves and Applications*).

[2] E. Somersalo, P. Ylä-Oijala and D. Proch: Analysis of Multipacting in Coaxial Lines. *FAE08, IEEE Proceedings, PAC 95, pp. 1500-1502.*

[3] E. Somersalo, P. Ylä-Oijala, D. Proch and J. Sarvas: Computational Methods for Analyzing Electron Multipacting in RF Structures, *Particle Accelerators*, 1998, to appear.

Computing the Scattering Matrix for a Microstrip Structure by Surface Integral Equation with Triangular Basis Functions

Matti Taskinen
Rolf Nevanlinna Institute
P.O.Box 4 (Ylipistonkatu 5), FIN-00014 University of Helsinki, Finland
e-mail: Matti.Taskinen@RNI.Helsinki.FI
telephone: +358-9-191 22778, telefax: +358-9-191 22779

1 Microstrip structures

The field computation for microstrips belongs to the rapidly expanding area of computational problems in microwave passive structures where Maxwell's equations are treated in a wide frequency range ($0 < f \leq 30GHz$). The microstrip structures are used for signal processing e.g. in mobile telephones. In this talk we present the field equation for microstrip, its numerical treatment, computing the scattering matrix, and also present some numerical examples. The talk is based on the joint research on microstrip field computation of Rolf Nevanlinna Institute and Nokia Research Center.

A microstrip structure consists of thin copper strips in one or several levels separated by dielectric layers, and of several feed lines and ports. In this talk we only consider one-layer structures with coaxial ports: the general case is treated in a similar way. We also only consider the time-harmonic case with fixed frequencies ($f > 0$) with time factor $e^{-i\omega t}$; the time-dependent signals can then be treated with Fourier transformation in time. In figure 1 there are two microstrip structures (above and side view). The second structure has three microstrips Ω_1, Ω_2 and Ω_3 and a coaxial feed line and port K.

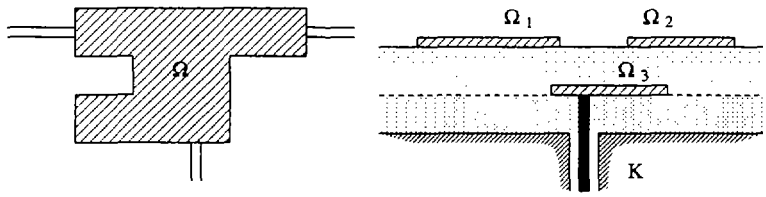

2 Scattering matrix

In a coaxial feed line the signal propagates in TEM mode and is determined by (alternating) voltage $V(z)$ and current $I(z)$, $z \geq 0$, as follows

$$V(z) = Ae^{i\beta z} + Be^{-i\beta z}, \quad I(z) = \frac{1}{Z_0}\left(Ae^{i\beta z} - Be^{-i\beta z}\right). \tag{1}$$

where $A, B \in \mathbf{C}$ are the complex amplitudes of the input and output (or scattered) signals, respectively, $\beta > 0$ is the propagating constant, and Z_0 is the characteristic impedance of the line. The port is the point $z = 0$ on the line. If $A_1, \ldots, A_P$ and $B_1, \ldots, B_P$ are the signal amplitudes at P ports and $Z_0^1, \ldots, Z_0^P$ are the characteristic impedances, then

$$\left[\frac{B_1}{\sqrt{Z_0^1}}, \ldots, \frac{B_P}{\sqrt{Z_0^P}}\right]^T = S\left[\frac{A_1}{\sqrt{Z_0^1}}, \ldots, \frac{A_P}{\sqrt{Z_0^P}}\right]^T \tag{2}$$

where S is the scattering matrix of the structure, and T stands for transpose.

For computing S we set a source at the q:th port, $1 \leq q \leq P$, with strength $A_q = Z_0^q$, and leave other ports open, i.e., $A_p = 0$ for $p \neq q$. Then we compute the currents I_p, $1 \leq p \leq P$ at

all ports, and by (1) and (2) obtain the q:th column of S from the resulting equation:

$$(3) \qquad -\left[\sqrt{Z_0^1}I_1,\ldots,\sqrt{Z_0^{q-1}}I_{q-1},\sqrt{Z_0^q}(I_q-1),\sqrt{Z_0^{q+1}}I_{q+1},\ldots,\sqrt{Z_0^P}I_P\right]^T = \sqrt{Z_0^q}S\,e_q,$$

where $e_q = [0,\ldots,0,1,0,\ldots,0]^T$ is the unit vector with 1 at the q:th position.

3 The field equation for computing the currents

For computing the currents $I_1,\ldots,I_P$ we also need to compute the induced surface current J_Ω on the microstrip Ω and the currents on coaxial probes at the ports. The current $J_\Omega \approx \sum a_n u_n$ is presented by triangular basis functions $u_n, n = 1,\ldots,N$, on Ω associated to a triangular grid on Ω, so that for each neighboring pair of triangles T_1, T_2 with a joint edge, there is one basis function u_n defined by

$$(4) \qquad u_n(x) = \epsilon_j(x - y_j), x \in T_j, j = 1,2,$$

where $\epsilon_1 = 1$ and $\epsilon_2 = -1$, and $y_j \in T_j, j = 1,2$ are the vertices of T_j opposing the joint edge. The currents on the probes are presented by special attachment functions v_n which model the current flow from the probe into Ω. Besides the fields due to currents, we also have fringe fields emerging from the coaxial port openings. They are modeled to be due to magnetic solenoids (frills) at ports with magnetic currents $V_p K_p, 1 \le p \le P$, where V_p is the voltage and K_p is a unit magnetic frill at the p:th port.

The physical field condition for our problem is that the tangential component of the total electric field must vanish on metallic surfaces. If we denote by $E(J)$ and $E(K)$ the tangential electric fields due to the tangential electric current J and magnetic current K and use (1), we can now write the field equation as follows:

$$(5) \qquad \sum_{n=1}^{N} a_n E(u_n) + \sum_{p=1}^{P} I_p\,[E(v_p) - Z_0^p E(K_p)] = -2Z_0^q E(K_q),$$

for the unknown coefficients $a_1,\ldots,a_N$ and unknown currents $I_1,\ldots,I_P$. The fields $E(u_n)$ are computed from the formula

$$(6) \qquad E(u_n)(x) = grad \int_\Omega G_v(x-y)\,div\,u_n(y)\,dy + \int_\Omega G_a(x-y)\,u_n(y)\,dy,$$

where G_v and G_a are Green's functions for the scalar and vector potentials of the electric field due to a surface current on Ω in the given layer structure. Functions G_v and G_a must be computed numerically which is a difficult task due to singularities and the associated oscillating and slowly converging Bessel integrals. Here we have used the new Matrix Pencil method for handling the integrals. The fields $E(v_p)$ and $E(K_p)$ are computed in a similar way.

The equation (6) is treated numerically by Galergin's method using $u_1,\ldots,u_N$ and $v_1,\ldots,v_P$ as test functions.

4 Computing the system matrix M

The most time-consuming part of the numerical solution is the computing of the system matrix M because of the numerical integrations. After streamlining the numerical algorithms for integration, one can still save great deal of time by observing that if two mesh triangle pairs are congruent, i.e. they are equal up to planar translations, rotations or reflections, they yield equal integrals to M. Therefore, we have also built a special mesh generator for the triangulation of Ω which leads to a mesh with a high number of congruent pairs. Also another program is constructed which finds the congruent pairs in a given triangulation. With these preprocessing programs the computing time of the system matrix is in some cases decreased to less than 1% of the original one.

Computational Analysis of an Open Magnetic Shield

Kimmo Forsman
Tampere University of Technology, Laboratory of Electricity and Magnetism, P.O. Box 692, FIN-33101 Tampere, Finland

Risto J. Ilmoniemi
BioMag Laboratory, Medical Engineering Centre, Helsinki Univ. Central Hospital, P.O. Box 508, FIN-00029 HYKS, Finland

I. Introduction

The most common method to obtain magnetic shielding, e.g., for biomagnetic measurements, is to use materials with high permeability and/or materials with high conductivity [1]. Typically, magnetically shielded rooms (MSR) have massive multilayered closed walls. We propose a new type of open magnetic shield of quite simple structure (and thus of low cost). Ideally, this structure would allow an infinite shielding factor at the center with a material of finite permeability.

II. Open Magnetic Shield

This magnetic shield consists of two sets of four ferromagnetic plates around the shielded region such that the closer plates are connected by rods to the outer plates at the opposite side of the shield. The centers of the plates are located at the vertices of two regular tetrahedra of different size. As the structure is therefore symmetric with respect to the four directions perpendicular to the plates, only one case when the external field is perpendicular to one pair of the plates need be analyzed. An example of this kind of shield is shown in Fig. 1.

III. Hybrid-Formulation Analysis

This shield is analyzed using a magnetostatic h-oriented hybrid formulation [2]. In a bounded domain Ω, including all magnetic material but no currents, the h-oriented hybrid formulation with an implicit Dirichlet boundary condition is: find the magnetic field $\mathbf{H} \in G^+$ such that

$$\int_\Omega \mathbf{H}' \cdot \mu \mathbf{H} \, dv = 0 \qquad \forall\, \mathbf{H}' \in G^0 \quad \text{and} \tag{1}$$

$$\mathbf{H} \times \mathbf{n} - \mathbf{H}^m(\chi \mathbf{H}) \times \mathbf{n} = \mathbf{H}^s \times \mathbf{n} \quad \text{on } \Gamma, \tag{2}$$

where Γ is the boundary of Ω, $\mathbf{n}$ is the unit normal vector of Γ, and $\mathbf{H}^s$ and $\mathbf{H}^m$ are the magnetic fields due to external sources and magnetization, respectively. Space G^+ consists of curl-free fields and $G^0 = \{\mathbf{u} \in G \,|\, \mathbf{u} \times \mathbf{n} = 0 \text{ on } \Gamma\}$, where G is the space of gradients. The hybrid formulation is discretized by using Whitney edge elements and the spanning-tree technique in a tetrahedral mesh.

The hybrid method suits well for this kind of problems, since a relatively small part of the system need to be modeled and the region where we want to know the magnetic field accurately is in air quite far away from the magnetic regions. Because of the rotational symmetry of this problem, only one third of the system need be modeled.

Kimmo Forsman, e-mail forsman@cc.tut.fi
Risto J. Ilmoniemi, e-mail rji@biomag.helsinki.fi

We studied the effects of the shield parameters on the performance of the shield, and different ways to apply the proposed shielding principle. As an example, the magnetic flux density $|\mathbf{B}|$ at the center of the shield of Fig. 1 in an external field $B_z = 1$ T is shown in Fig. 2. The shielding factor is over 100 in a center region of about 20 cm in diameter, the open-volume diameter being 100 cm. In some parts of the shielded region (e.g., on the z-axis) $\mathbf{B}$ is in opposite direction with respect to the external field.

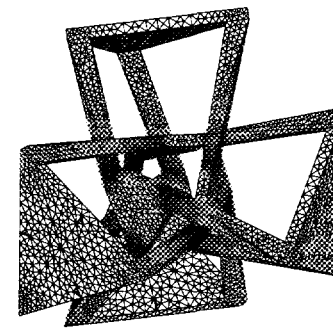

Fig. 1. Open magnetic shield with the mesh used in the analysis.

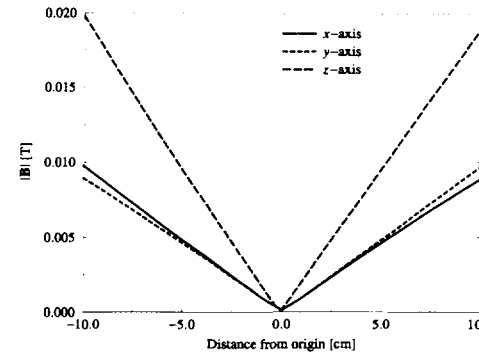

Fig. 2. Magnetic flux density $|\mathbf{B}|$ at the center of the shield along the coordinate axes when the external field is $B_z = 1$ T. The distance from origin to the nearest magnetic plates is 50 cm.

References

[1] V. O. Kelhä, J. M. Pukki, R. S. Peltonen, A. J. Penttinen, R. J. Ilmoniemi, and J. J. Heino, "Design, construction and performance of a large-volume magnetic shield," *IEEE Trans. Magn.*, vol. 18, pp. 260–270, 1982.

[2] K. Forsman, J. Kangas, J. Salonen, A. Arkko, and L. Kettunen, "Properties of 3D magnetostatic hybrid formulations," *IEEE Trans. Magn.*, 1998. In press, (also in Compumag-Rio 1997).

ON ELECTROMAGNETIC FORCE COMPUTATION

Aapo Koski, Kimmo Forsman, Timo Tarhasaari, Jari Kangas
and Lauri Kettunen
Tampere University of Technology, Laboratory of Electricity and Magnetism
P.O.Box 692, FIN-33101 Tampere, Finland

Introduction

The force resulting from an electromagnetic interaction is of fundamental importance for a majority of engineering problems. Thus any method for computing the magnetic field is of practical value only if it is accompanied with an accurate and sufficently fast method for the force evaluation. Ideally, forces or torques should be obtainable directly without any further interaction or excessive manipulation of the field solution.

Alternatives for Force Computation

Basically, the alternatives for calculating the total electromagnetic force acting on a body are the three traditional methods: the Maxwell's Stress tensor (MST), the magnetic energy variation (or the virtual work) and the equivalent sources methods.

1. **Maxwell's Stress Tensor:** The MST is based on the fact that the field inside a closed surface in free space remains unchanged if the field sources external to the surface are replaced by equivalent sources on the surface. The total force may then be calculated by an integration of the force density over a closed surface enclosing the region. Theoretically, the chosen integration surface is arbitrary, i.e. we should end up with the same answer regardless of what closed surface is selected. In practice, however, the force computed depends heavily on the placement of the integration surface in the space and the force density suffers from large numerical errors, especially near sharp corners of the model. Usually MST results are most reliable when the integration surface is relatively far away from any active material boundary and trial and error is used to find the number and distribution of grid points on the surface for force density evaluation.

Thus, there are two main drawbacks with MST: (1) it does not give reliable results without user interaction, and (2) a time consuming integration procedure is required.

2. **Virtual Work:** To use the magnetic energy variation method for force computation we need to be able to derive the total magnetic energy of the system.

Ren and Razek [2] have proposed one idea for local force computation using virtual work. In that method only one field solution is required and the results they obtained were encouraging. However, the local energy density can be computed accurately only for inner nodes of the mesh and thus an extra layer of elements is required on the active material boundary for some formulations.

3. **Equivalent Currents:** The equivalent source method is based on replacing the magnetization m by an equivalent current density $j^m = \text{curl}\, m$ and an equivalent surface current density $k^m = m \times n$. After this replacement the field can be described solely by the current density distribution $\hat{j} = j + j^m$ and surface current distribution k^m. The current density j includes both the source currents j^s and the induced eddy currents σe.

The force density on a current carrying body may be computed by integrating the force density $f = \hat{j} \times b^*$ over the target body. The difference between b^*- and b-field is that source of b^* is $\hat{j}$ supported in the space outside the target body whereas b is due to $\hat{j}$ supported in whole space.

Using b^* instead of b is justified by two facts: (1) a current carrying element does not exert any force on itself, and (2) by Newton's III law the total force exerted by a set of current carrying elements on itself within a rigid body is zero. What is gained is a reduction in the sources of error in the obtained results, and in solution time.

Equations of Motion

The translation of a body of mass m is governed by Newton's II law $F = m\partial_t v$, where v is velocity of the center of gravity. The total force F includes all the forces acting on the body, magnetic, mechanical and gravitational forces.

The change in the orientation of a rotating body in a local reference frame at r' is obtained from its angular velocity ω in a fixed coordinate frame. ω is related to the torque by $(r - r') \times F = \partial_t (J\omega) + B\omega$, where J is moment of inertia and B mechanical damping coefficient.

References

[1] A. Koski, K. Forsman, T. Tarhasaari, J. Kangas and L. Kettunen "Force and Torque Computations with Hybrid Methods," in *IEEE CEFC'98 – Tucson*, June 1998.

[2] Z. Ren and A. Razek "Local force computation in deformable bodies using edge elements," *IEEE Trans. Magn.*, vol. 28, pp. 1212–1215, March 1992.

Variable Step Size Runge-Kutta Methods and Eddy Current Problems

Frank Cameron and Kimmo Forsman
Tampere University of Technology, P.O. Box 692, 33101 Tampere, Finland
email: frank@cc.tut.fi

I. Introduction

Common numerical approaches to solving nonlinear transient electromagnetic field (i.e. eddy current) problems yield initial value problems (IVP) of the form

$$\mathbf{S}(\cdot)\,\dot{\mathbf{y}} \;=\; \mathbf{R}(\mathbf{y})\,\mathbf{y} + \mathbf{f}(t)\;, \quad \mathbf{y}(t_0) = \mathbf{y}_0\;, \tag{1}$$

after spatial discretisation. In (1) $\mathbf{f}(t)$ is a driving function. The choice of an appropriate time integration method for (1) depends on the properties of $\mathbf{S}$ [1],[2]. What makes eddy-current problems challenging is that $\mathbf{S}$ is singular, i.e. (1) is not an ODE but rather a differential-algebraic equation set (DAE). This in turn implies that time integration methods designed for ODEs may not be appropriate.

An important issue in time integration schemes is whether the time step size h is constant or variable. Our purpose is to discuss some issues related to varying h — some purely computational, others related to the electromagnetic problem being solved.

II. Runge-Kutta methods

We use time integration methods belonging to the Runge-Kutta (RK) family. An s stage RK method is specified by an $s \times s$ matrix $\mathbf{A}$ and $s \times 1$ vector $\mathbf{b}$. Starting from the initial condition $\mathbf{y}_n$ at t_n the ith stage of an RK method is defined by

$$\mathbf{Y}_i = \mathbf{y}_n + h \sum_{j=1}^{s} a_{ij} \mathbf{Y}'_i\;. \tag{2}$$

The stage values are obtained by substituting $\mathbf{Y}_i$ for $\mathbf{y}$ and $\mathbf{Y}'_i$ for $\dot{\mathbf{y}}$ in (1) and solving the resulting equation set. For this equation set to be solvable we must use implicit RK methods, i.e. methods where $\mathbf{A}$ is invertible. For example, applying backward-Euler to (1) and assuming $\mathbf{S}$ depends on $\mathbf{y}$ yields

$$\mathbf{S}(\mathbf{Y})\,(\mathbf{Y} - \mathbf{y}_n) \;=\; h\,\mathbf{R}(\mathbf{Y})\,\mathbf{Y} + h\,\mathbf{f}(t_n + h) \tag{3}$$

When all stages have been computed the state is advanced using

$$\mathbf{y}_{n+1} = \mathbf{y}_n + h \sum_{i=1}^{s} b_i \mathbf{Y}'_i\;. \tag{4}$$

An *embedded pair* of RK methods is typically used to estimate the error in $\mathbf{y}$. Such a pair uses the same $\mathbf{A}$ matrix but different advancing vectors $\mathbf{b}$ and $\widehat{\mathbf{b}}$. Assuming $\widehat{\mathbf{b}}$ corresponds to the more accurate RK method then an estimate of the error in $\mathbf{y}$ from (4) is

$$\mathbf{e} = h \sum_{i=1}^{s} (b_i - \hat{b}_i) \mathbf{Y}'_i\;. \tag{5}$$

III. Computational issues

A. Error control

The main reason for allowing varying h is to have some means for controlling the error incurred in discretizing time. By varying h we can control the error estimated by (5), which is clearly an advantage over constant h schemes. Varying h schemes however are more difficult to design and implement [3]. For example in a constant h scheme we need design only one $\mathbf{b}$, whereas in a varying h scheme we need both $\mathbf{b}$ and $\widehat{\mathbf{b}}$.

B. Interpolation

When using a varying h scheme the times when y is estimated depend on several factors: the step size controller used, the required accuracy, the dynamics of the system being simulated, etc. Often however we want to give the time when y is estimated, e.g. at fixed time intervals. We could of course take the $(t_n, \mathbf{y_n})$, $n = 0, 1, \ldots, N$ and perform post-run interpolation, e.g. using splines. For RK methods there is an alternative, we can form RK interpolators, also known as continuous extensions [5]. Such interpolators are commonly written as

$$\mathbf{y}(\sigma) = \mathbf{y}_n + \sigma h \sum_{i=1}^{s} b_i(\sigma) \mathbf{Y}'_i\;. \tag{6}$$

where $0 \le \sigma \le 1$. The coefficients $b_i(\sigma)$ must be designed beforehand. For RK methods suitable for eddy-current problems the estimates provided by an RK interpolators (4) is typically of a lower order, i.e. less accurate, than the RK method used to advance the state (4).

C. Linear solvers

Regardless of whether eddy current problem (1) is linear or non-linear, during time integration we will have to solve several linear systems. For simplicity we will consider the

case where (1) is linear and we are using backward Euler. From (3), we want to find $\mathbf{Y}$ from

$$(\mathbf{S} - h\mathbf{R})\mathbf{Y} = \mathbf{S}\mathbf{y}_n + h\,\mathbf{f}(t_n + h) \tag{7}$$

There are two families of methods for solving (7): (i) direct solvers, *i.e.* LU or some variant, and (ii) iterative solvers, e.g. CG, GMRES, BiCGStab. With regard to (i) the following must be taken into account when considering varying h:

1. When h is changed, $(\mathbf{S} - h\mathbf{R})$ in (7) must be refactored.
2. Once $(\mathbf{S} - h\mathbf{R})$ has been factored, solving (7) for new right hand sides is fairly inexpensive.

It follows that when using direct solvers step size controllers must often resolve conflicting objectives [3, sec. 5.3]: (i) avoid changing h so as to reduce the number of matrix factorizations, (ii) change h so as advance as quickly as possible while retaining given tolerances on the error.

With regard to iterative solvers (ii) the following must be taken into account:

1. Given that we have solved (7), typical iterative methods do not have much information that can be carried forward and used to advantage when solving (7) with a new right hand side.
2. Termination tolerances must given to the iterative solver. These tolerances should ensure that the solution of (7) is at least as accurate as the accuracy we are requiring from our RK method, but is not excessively over-accurate [4].

IV. Electromagnetic issues

A. B-formulations

One formulation for setting up the IVP (1) is the B-formulation in which Faraday's law, Gauss's law, and the constitutive laws are imposed exactly and Ampère's law holds in the weak sense. One consequence of the B-formulation is that to obtain eddy currents we need to estimate $\dot{\mathbf{y}}$ in addition to estimating $\mathbf{y}$. With a certain class of RK methods, estimates for $\dot{\mathbf{y}}$ can be easily obtained at the time instants when $\mathbf{y}$ is estimated. However, while it is possible to obtain RK interpolators for $\mathbf{y}$, it is an open question of whether good RK interpolators exist for $\dot{\mathbf{y}}$. As discussed in section III., with varying h it is important to have an interpolators so as to obtain estimates at the time we desire, not simply at the times the step-size controller happens to choose.

We could simply augment (1) by letting $[\mathbf{v}^\mathbf{T}, \mathbf{w}^\mathbf{T}] = [\mathbf{y}^\mathbf{T}, \dot{\mathbf{y}}^\mathbf{T}]$, which would result in

$$\begin{bmatrix} \mathbf{I} & 0 \\ 0 & 0 \end{bmatrix} \begin{bmatrix} \dot{\mathbf{v}} \\ \dot{\mathbf{w}} \end{bmatrix} = \begin{bmatrix} 0 & \mathbf{I} \\ \mathbf{R} & -\mathbf{S} \end{bmatrix} \begin{bmatrix} \mathbf{v} \\ \mathbf{w} \end{bmatrix} + \begin{bmatrix} 0 \\ \mathbf{f}(t) \end{bmatrix} \tag{8}$$

One drawback of this is that we need twice as much storage, since we have doubled the number of states.

B. Control of global quantities

In simulating eddy current problems we are often interested in some global property that is a function of the states. For example, for an H-formulation the power P can be written as

$$P = \mathbf{y}^\mathbf{T}\mathbf{M}\mathbf{y} \tag{9}$$

where $\mathbf{M}$ is a matrix that depends on the spatial discretization. The advantage of having varying h being used to control error is that we can control the error in P by appending equation (9) to (1) and adding one state, i.e. P. The fact that (9) is an algebraic equation does not cause problems since (1) is a DAE already.

References

[1] F. Cameron, *On low-order DIRKs and DAEs*, submitted, 1998.

[2] F. Cameron, R. Piché, and K. Forsman, *Variable step size time integration methods for transient eddy current problems*, IEEE Trans. Magn. (1998) in press.

[3] K. Gustafsson, *Control of Error and Convergence in ODE Solvers*, Ph.D. Thesis, Lund Institute of Technology (1992).

[4] C.T. Kelley, *Iterative Methods for Linear and Nonlinear Equations*, SIAM, Philadelphia, (1995).

[5] Shampine, L.F. *Numerical solution of ordinary differential equations*. Chapman and Hall, New York, 1994.

Hybrid Formulations and Time Harmonic Eddy Current Problems

Jussi Kaisjoki, Kimmo Forsman and Lauri Kettunen
Tampere University of Technology, Laboratory of Electricity and Magnetism,
P.O. Box 692, FIN-33101 Tampere, Finland. e-mail: kaisjoki@cc.tut.fi

I. Introduction

We introduce a hybrid formulation for solving linear time harmonic eddy current problems in 3D in terms of the magnetic field h. The corresponding method for transient eddy current problems is presented in [1] and the theoretical background for this approach (e.g. discretization and multiply connected regions) is discussed in more detail in [2]. In this paper we concentrate on the time harmonic case and its efficient implementation. Some test results are shown to verify the proposed method.

II. Hybrid Formulation

The bounded 3D domain Ω is allowed to be multiply connected and its boundary is denoted by Γ. All conducting and magnetic material and no source currents j^s are assumed to lie inside Ω. Thus the hybrid h-formulation with an implicit Dirichlet boundary condition is in the time harmonic case: find complex $h \in \mathbb{L}^2(\Omega)$ such that

$$\int_\Omega h' \cdot \mu h \;=\; 0 \qquad \forall\, h' \in G^0\,, \tag{1}$$

$$h \times n - H(\operatorname{curl} h, \chi h) \times n = h^s \times n \quad \text{on } \Gamma \text{ and} \tag{2}$$

$$\int_\Omega \operatorname{curl} h' \cdot \frac{1}{\sigma} \operatorname{curl} h + \mathrm{i}\omega \int_\Omega h' \cdot \mu h + \mathrm{i}\omega \int_\Gamma h' \times A(\operatorname{curl} h, \chi h) \cdot n$$
$$= \; -\mathrm{i}\omega \int_\Gamma h' \times a^s \cdot n \qquad \forall\, h' \in \mathbb{L}^2_{\operatorname{curl}}(\Omega)\,, \tag{3}$$

where n is the unit normal of Γ, i is the imaginary unit and ω is the angular frequency. The integral operators H and A yield the h and a-fields (a is the magnetic vector potential) due to the currents ($\operatorname{curl} h$) and magnetization (χh) and these fields are denoted by $H(\operatorname{curl} h, \chi h)$ and $A(\operatorname{curl} h, \chi h)$, respectively. The fields due to j^s are called h^s and a^s. Furthermore, G^0 and $\mathbb{L}^2_{\operatorname{curl}}(\Omega)$ are subspaces of space $\mathbb{L}^2(\Omega)$ of square-integrable vector fields over Ω such that $G^0 = \{u \,|\, \operatorname{curl} u = 0, u \times n = 0 \text{ on } \Gamma\}$ and $\mathbb{L}^2_{\operatorname{curl}}(\Omega) = \{u \,|\, \operatorname{curl} u \in \mathbb{L}^2(\Omega)\}$. This hybrid approach is discretized by using Whitney edge elements and the spanning-belted-tree technique in a tetrahedral mesh. [1],[2]

We shall discuss how the structure of the resulting system of equations — a sparse matrix with a (almost totally real) dense block — can be utilized in iterative solvers and thus obtain good perfomance. In addition different options for achieving efficient implementation of the integral operators will be discussed.

III. Test Problem

The method is validated with TEAM Workshop problem 7 which consists of an asymmetrical aluminum plate with a hole [3]. The exciting field is produced by a coil with a sinusoidal current (f = 50 Hz). Figure 1 shows the mesh and the computed eddy current solution. The number of complex degrees of freedom is 5299.

In Figure 2 the z-component of magnetic flux density b is calculated. A good correspondence with the measured values and with other computed results is obtained [3].

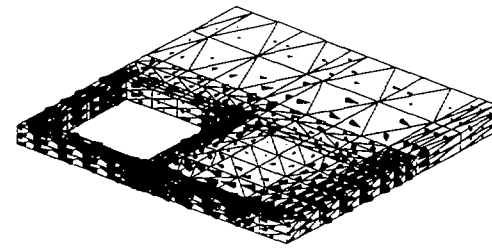

Fig. 1. The computed eddy currents at $\omega t = 0$.

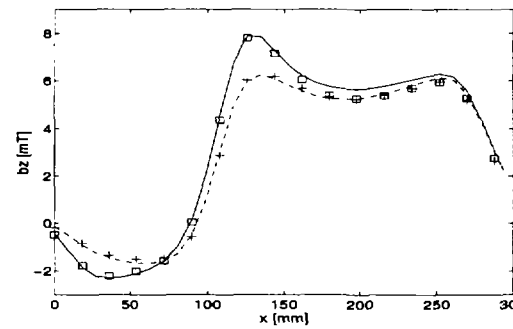

Fig. 2. Comparison of computed b_z at $\omega t = 0$ along the line y = 72 mm, z = 34 mm (the solid line) and along the line y = 144 mm, z = 34 mm (the dashed line) and measured b_z [3], marked with squares and plusses, respectively.

References

[1] K. Forsman and L. Kettunen, "Hybrid formulations for 3D magnetostatic and eddy current problems," *ACES Journal*, vol. 12, pp. 140–144, July 1997.

[2] L. Kettunen, K. Forsman, and A. Bossavit, "Formulation of the eddy current problem in multiply connected regions in terms of h," *Int. J. Numer. Meth. Engng.*, vol. 41, pp. 935–954, 1998.

[3] K. Fujiwara and T. Nakata, "Results for benchmark problem 7 (asymmetrical conductor with a hole)," *COMPEL*, vol. 9, no. 3, pp. 137–154, 1990.

TWO-DIMENSIONAL INVERSION OF VLF DATA IN GEOPHYSICAL EXPLORATION

Pirttijärvi M., Kaikkonen P., Sharma S. P. and Hjelt S.-E.

Dept. of Geophysics, University of Oulu, 90570, Oulu

For over three decades the VLF method has been used for various geophysical investigations, such as environmental studies, structural mapping as well as mineral exploration. Unfortunately, the interpretation is often left at qualitative stage and the information content of the VLF data is not fully utilized. However, the recent advances in numerical methods and computer technology have made it possible to develop practical interpretation programs for microcomputer environment.

We have developed an inversion program for the interpretation of VLF and VLF-R data. The direct computation is based on integral equation method, where a two-dimensional (2-D) model under E-polarization mode is considered (Nissen, 1985). The interpretation method is based on linearized inversion where the singular value decomposition (SVD) and an adaptive damping method is used (Pirttijärvi et al., 1998). The model consists of dyke-like bodies embedded in conductive two-layer host. The parameters of the model are: the resistivity (RL) and the thickness (TL) of the overburden, the resistivity of the host (RH) and the x-location (X0), depth to the top (DB), width (W), height (H), dip angle (D) and the resistivity (RB) of each body.

The performance of the inversion method is demonstrated using both synthetic and field data. Additional information given by the SVD-analysis about the resolution of the model parameters is also shown.

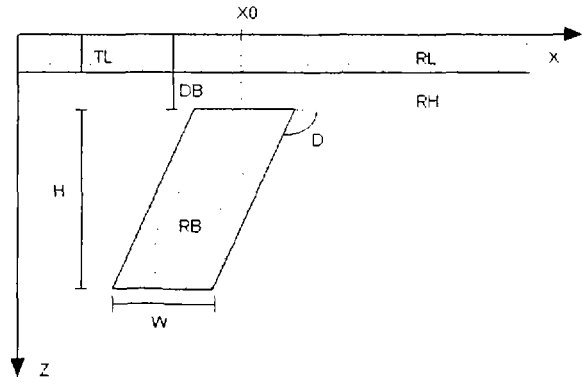

Figure 1. *The parameters of the dipping dyke model.*

References

Nissen, J., 1985: Ph.D thesis, *Versatile programs for the geoelectromagnetic interpretation*. Luleå University, Sweden.

Pirttijärvi, M., Verma, S.K. and Hjelt, S.-E., 1998. *Inversion of transient electromagnetic profile data using a conductive finite plate model*. J. Appl. Geophys., 38, 181–194.

Effective permittivity of a dielectric mixture calculated by FDTD method

Kimmo Kärkkäinen, Olli Pekonen*, Ari Sihvola, and Keijo Nikoskinen
Electromagnetics Laboratory, Helsinki University of Technology
P.O. Box 3000, 02015 HUT
* Nokia Telecommunications, Radio Network Tools
P.O.Box 311, FIN-00045 Nokia Group, Finland
e-mail: Kimmo.Karkkainen@hut.fi

Abstract – The present paper reports the results of an extensive numerical analysis of electromagnetic fields in random dielectric material mixtures. The effective permittivity of the medium is calculated by FDTD simulations of such a sample in a TEM-waveguide.

The history of the study of heterogeneous mixtures dates back to 19th century, and several empirical and analytical models for the effective properties of mixtures have been proposed. However, the problem has been approached with computational means only recently [1], [2]. This paper demonstrates an approach for solving the characteristics of a heterogeneous lossless two-phase mixture numerically by means of the well-known FDTD method. The simulations are carried out in two-dimensional computational space where two dimensional spheres (cylinders) are embedded. The effective permittivity of the material is deduced from the reflection behavior at the surface of the mixture which is placed into a TEM parallel plate waveguide. The simulation domain is seen in Fig. 1. The effective permittivity of the mixture becomes available from the

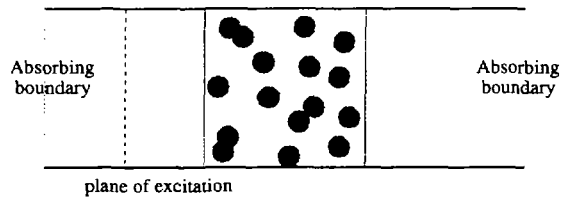

Figure 1: Simulation domain

reflection coefficient by simple transmission line analogy. Based on the transmission line theory, the absolute value of the reflection coefficient acting at the left boundary of the slab is

$$|R| = \left| \frac{Z_1 - Z_0}{Z_1 + Z_0} \right|, \tag{1}$$

where Z_0 is free space impedance $\sqrt{\mu_0/\epsilon_0}$ (this is also applicable to the TEM waveguide), and Z_1 the "input impedance" of the slab/free space system. If the width of the slab is w and effective relative permittivity is ϵ_{eff} then

$$Z_1 = Z_0 \frac{1 + j\epsilon_{\text{eff}}^{-1/2} \tan(kw)}{1 + j\epsilon_{\text{eff}}^{1/2} \tan(kw)}, \tag{2}$$

where $k = \frac{2\pi f}{c_0} \epsilon_{\text{eff}}^{1/2}$. From (1) and (2) one obtains following transcendental equation for the effective relative permittivity:

$$|R| + \frac{\tan(\frac{2\pi f w}{c_0} \epsilon_{\text{eff}}^{1/2})(\epsilon_{\text{eff}} - 1)}{\sqrt{4\epsilon_{\text{eff}} + \tan^2(\frac{2\pi f w}{c_0} \epsilon_{\text{eff}}^{1/2})(\epsilon_{\text{eff}} + 1)^2}} = 0. \tag{3}$$

Thus, by knowing the absolute value of the reflection coefficient one is able to estimate the effective relative permittivity by numerically solving the equation (3).

Several simulations with random inclusion distributions are carried out in order to obtain average properties of a mixture having certain inclusion volume fraction. Clustering of the circular inclusions is allowed. In Fig. 2 the simulation results and well-known classical mixing rules are compared in the case where inclusion permittivity is 16 times the environment permittivity and vice versa.

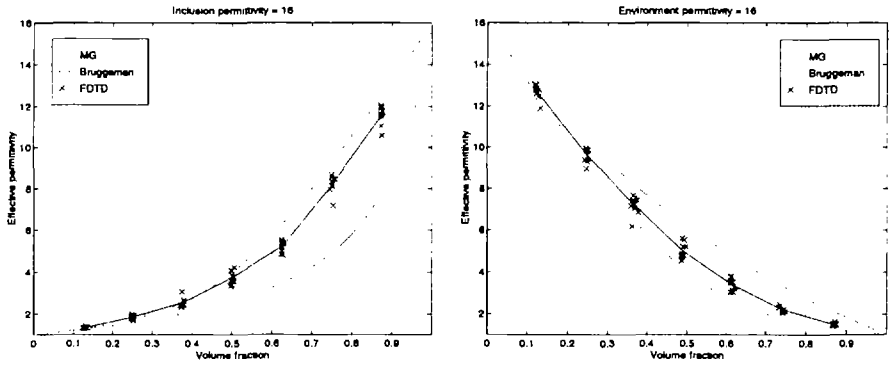

(a) Raisin $\epsilon_i > \epsilon_e$ (b) Cheese $\epsilon_i < \epsilon_e$

Figure 2: Relative effective permittivity of a mixture with material contrast 16. Legend: MG - Maxwell Garnett formula; Bruggeman - effective medium formula; FDTD - FDTD simulation results for random inclusion distributions

References

[1] Leslie Greengard, Monique Moura: "On the numerical evaluation of electrostatic fields in composite materials",*Acta Numerica*,, 1994, pp. 379-410

[2] B. Sareni, L. Krähenbühl, A. Beroual, C. Brosseau:"Effective dielectric constant of periodic composite materials".*Journal of Applied Physics*, 1996, volume 80, number 3, pp. 1688-1696

SOFTWARE FOR ENUMERATION OF EFFECTIVE PARAMETERS FOR CHIRAL AND BI-ANISOTROPIC MATERIALS

Juha Avelin and Ari Sihvola
Electromagnetics Laboratory, Helsinki University of Technology
P.O. Box 3000, FIN-02015 HUT, Finland
Fax: + 358-9-451 2267; email: sakke@eml.hut.fi, ari@eml.hut.fi

Abstract

A software package is being developed for the analysis of complex heterogeneous materials, including chiral, bi-isotropic, and bi-anisotropic media. The programme calculates the effective magnetoelectric material parameters as functions of the structure and geometry of the mixture.

One of the interesting topics in the electromagnetics community has been the modelling of complex materials, in other words the enumeration of the macroscopic parameters of a mixture that shows complex polarization mechanisms in the small scale. Several types of mixing formulas and homogenization principles have been proposed for chiral and even bi-anisotropic materials.

The present contribution reports a numerical effort, to capture the power of the various electromagnetic mixing rules into a single and user-friendly computer programme.

The mixing rules implemented numerically in the software—which is called *Mixtool*—predict the effective permittivity, permeability, and the two magnetoelectric parameters (which can be scalars in the isotropic case, complex in the lossy case, dyadics/matrices in the anisotropic and bi-anisotropic cases) as functions of the geometry and the primary magnetoelectric parameters of the inclusions. *Mixtool* uses the famous mixing models, for example Maxwell Garnett, Bruggeman and Coherent Potential model. The analysis is making use of the unified mixing rule where all these models are seen as members of family of mixing rules with a parameter *v*. *Mixtool* uses an accurate function—based on elliptic integrals—to calculate the depolarization factors of ellipsoids.

The ellipsoids can be aligned or randomly oriented or they can have an orientation distribution, which can be determined by a distibution function or rose diagram. Ellipsoids can even be layered, consisting of two layers.

If the background material is anisotropic, usual mixing formulas can be used, if the background material is transformed to isotropic material using affine transformation.

In *Mixtool* there is a graphical, userfriendly interface. On the right edge of the main window there are various buttons, with which the output of *Mixtool* can be controlled. One component of an electric parameter dyadic can be selected for plotting.

Figure 1 shows an example plot from an isotropic case, where $\epsilon_e = 1$ and $\epsilon_i = 10$. The inclusion material is in the form of spheres. Plotted are Maxwell Garnett, Bruggeman, and Coherent Potential models.

With the input window in Figure 2, the user of *Mixtool* can give the axes of ellipsoids, their orientation compared to the background and the orientation of eigenvectors of electric parameters. User can also give values to the whole material dyadic. The orientation of inclusions: random, aligned, rose diagram, etc., can also be given in this window.

An example of a chiral mixture is shown in Figure 3. There the inclusion and environment are mirror-image media of each other: their permittivities and

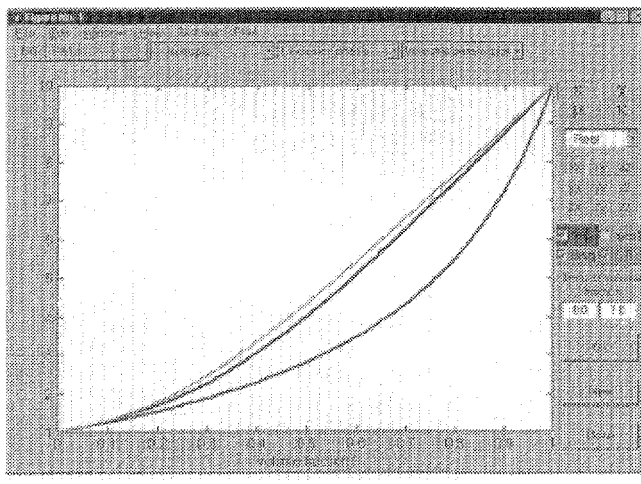

Figure 1. *The main window of Mixtool.*

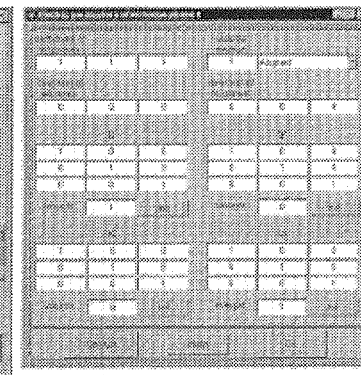

Figure 2. *The input window for parameters of the inclusion phase.*

permeabilities are the same, but the chirality parameters are opposite. In particular; $\epsilon_i = \epsilon_e = 2$, $\mu = 1.5$ and $\kappa_i = -\kappa_e = 1$. In the figure the curves show all the three basic mixing models. The effective chirality parameter of this mixture is seen to increase monotonously from the environment value to the inclusion value as the volume fraction increases from 0 to 1. The predictions of the various mixing principles differ, and among those, the Bruggeman rule is seen to cross the zero-chirality level at exactly $f = 0.5$.

Another example is a very lossy mixture, shown in Figure 4. The Maxwell Garnett plot shows the effective permittivity of isotropic, lossy case. ε_{eff} curves start from the environment value and reach the inclusion values for full mixing. But the real part of the effective permittivity increases strongly and shows a maximum: it peaks around the volume filling of 80%, after which is levels down to the inclusion value.

As a conclusion, *Mixtool* could be of much use for people interested in the effective properties of heterogeneous materials, including chiral and bi-anisotropic media.

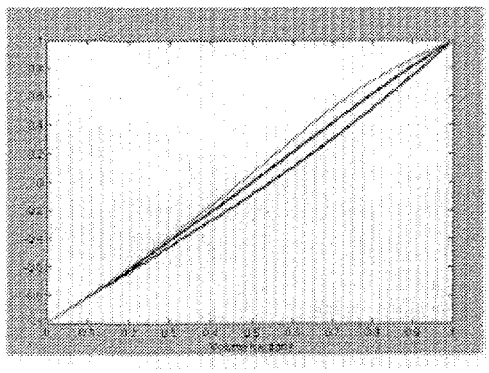

Figure 3. *The chirality parameter of a mirror-image mixture.*

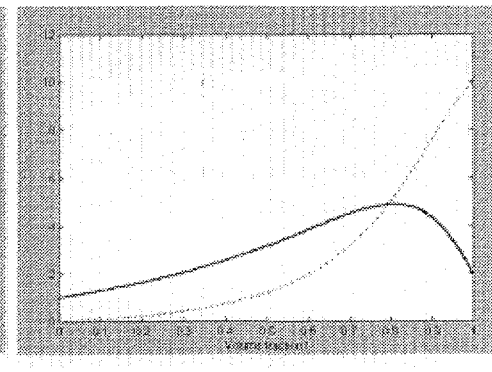

Figure 4. *The effective permittivity of a lossy mixture.*

GENERAL DESIGN APPROACH TO PHASE DIVERSITY ANTENNA ARRAYS

Juha Juntunen, Keijo Nikoskinen
Helsinki University of Technology, Institute of Radio Communications, Electromagnetics Laboratory,
P.O.Box 3000, FIN-02150 ESPOO, Finland
phone: +358 9 451 2260, fax: +358 9 451 2267
e-mail: Juha.Juntunen@hut.fi, Keijo.Nikoskinen@hut.fi

Diversity reception is a widely used technique in radio communications to alliviate signal fading due to multipath signal components caused by complex radio wave propagation environments, such as downtown areas in large cities. There exists many diversity techniques, which can be used to reduce the effect of fading in mobile communication networks. This presentation is focused on phase diversity array antennas, which could be utilized as base station antennas in cellular networks.

The emphasis of the presented analysis is on phase diversity properties of diversity arrays [1]. For every imaginable array geometry of two or more antenna elements, there are excitations which correspond to exactly the same amplitude pattern but dissimilar phase patterns. This condition can be considered as a special subspace in the full, arbitrary multidimensional space of array excitations. The existance of this subspace is the starting point in the following analysis of general phase diversity arrays. Phase diversity is an attractive form of antenna diversity, since the radiation pattern is completely independent of the chosen array excitations. The unchanging radiation pattern of a base station antenna assists network and frequency planning of mobile communication networks, since it is often necessary to minimize the interference from the neighboring cells of the base station.

Since the diversity in this case is a property of a group of antenna elements, the parameters allowing the design of diversity arrays are the amplitude and phase excitations and physical locations of antenna elements. In the most

simple case of antenna array, in which the array consists of only two antenna elements, the array factor describing the radiation properties of the array can be written as

$$f_{AF}(\theta) = 1 + I_1 e^{j(kd_1 \cos\theta + \delta_1)} \quad (1)$$

where the first term of the sum corresponds to the element at the origin and the second term is due to the other element, whose excitation is defined by the excitation current ratio I_1 and the phase difference parameter δ_1. The antenna elements are seperated by the distance d_1. k denotes the free space wave-number $k = 2\pi / \lambda = \omega\sqrt{\epsilon_0 \mu_0}$. The phase diversity qualities of the array can be observed, if one substitutes the current ratio parameter I_1 by its inverse

$$I_1 \rightarrow \frac{1}{I_1} \quad (2)$$

This change doesn't affect to the shape of the radiation pattern, even though the phase pattern of the array becomes altered.

This fundamental case of only two antenna elements can be used as a building block in design of more complex and general diversity arrays, and in the same time this approach reveals the phase diversity condition in terms of the chosen array geometry and excitation parameters. In this presentation it is shown how one can easily construct linear, planar or even full 3D-arrays whose phase properties are far more versatile than that of a two-element array and can be changed in the similar fashion as the radiation pattern shape stays unchanged.

The most self-evident application of this theory is in mobile communication networks where diversity reception is already used in it's most simple forms. The use of diversity arrays could easily be adopted to the present mobile communication systems to offer increased fading reduction performance.

[1] J. Lempiäinen, K. Nikoskinen, J. Juntunen. Multistate phase diversity microcell antenna. Electronic letters, Vol. 33, No. 6, pp. 438–440, March 1997.

CALIBRATION OF SAR PROBES IN WAVEGUIDE AT 900 MHz

Kari Jokela: STUK, PL 14, 00881 Helsinki, kari.jokela@stuk.fi
Petri Hyysalo: Mecrastor Coopers & Lybrand Ltd., Kimmeltie 3, 02110 Espoo, petri.hyysalo@mecrastor.fi
Lauri Puranen: STUK, PL 14, 00881 Helsinki, lauri.puranen@stuk.fi

The radiation safety tests for hand-held mobile phones require precise calibration of the small electric field probes used for the measurement of SAR in phantoms simulating the human body. In this study a calibration system based on a rectangular waveguide was developed for SAR calibrations at 900 MHz. The cross-sectional dimensions of the waveguide are a = 0.19 mm and b = 0.14 mm. The waveguide is loaded with a rectangular liquid slab where the dielectric parameters of the medium simulate human muscle and brain. The precise SAR reference is derived from the temperature rise during a short-term (10 to 15 s) microwave heating of the lossy slab by measuring with sensitive thermistor-type probes equipped with high resistance lines. The thermistor probes are calibrated against a calibrated mercury thermometer. To improve the uniformity of the electric field at the calibration position, the thickness of the tissue equivalent slab was varied to adjust the standing wave pattern. This resulted in an almost threefold reduction in the positioning error of the E-field probe. The absolute uncertainty of the calibration is estimated to be ± 5.6 % (2σ) not including the uncertainty of conductivity. The difference between the thermally measured SAR and a value computed with the FDTD method was well within this limit of uncertainty. Closed waveguide systems are more compact and require less microwave power than open field calibration systems. Moreover, no radio-frequency interference is generated.

Monikerrosrakenteen likipitävät impedanssireunaehdot

P. Puska, S. Tretyakov ja A. Sihvola
Sähkömagnetiikan laboratorio, Teknillinen korkeakoulu

1 Taustaa

Likipitävillä reunaehdoilla on jo kauan helpotettu reunaehto-ongelmien käsittelyä [1, 2]. Impedanssin avulla kirjoitettuna reunaehto, olipa tämä sitten tarkka tai likipitävä, ilmoittaa sähkö- ja magneettikentän suhteen reunalla ∂D, eli

$$\mathbf{E}|_{\partial D} = \overline{\overline{Z}}_{\mathrm{eq}} \cdot \mathbf{n} \times \mathbf{H}|_{\partial D}, \tag{1}$$

jonka voi myös ajatella esittävän magneettikentän kuvausta sähkökentälle lineaarioperaattorin $\overline{\overline{Z}}_{\mathrm{eq}}$ välittämänä. Ajattelemmekin vast'edes että impedanssi on operaattori. Ongelmamme on tämän operaattorin likiarvoistaminen.

2 Teoria

Uskomme siis, että mielivaltaisen n-kerrosrakenteen kenttien suhde ainakin paikallisesti määräytyy yhtälön (1) mukaan. Impedanssioperaattori on reunapinnan suhteen Fourier-muunnettuna [3]

$$\overline{\overline{Z}}_{\mathrm{eq}} = Z_{\parallel}\frac{\mathbf{k}_t\mathbf{k}_t}{k_t^2} + Z_{\perp}\frac{\mathbf{ww}}{k_t^2}. \tag{2}$$

missä $\mathbf{w} = \mathbf{n} \times \mathbf{k}_t$ ja $\mathbf{k}_t$ on aaltovektorin $\mathbf{k}$ reunan suuntainen osa. $Z_{\parallel}$ ja $Z_{\perp}$ yhdelle d:n paksuiselle kerrokselle ovat

$$Z_{\parallel} = \eta_1 \cos(\theta_1)\frac{Z_L + j\eta_1 \cos(\theta_1)\tan(\beta_1 d_1)}{\eta_1 \cos(\theta_1) + jZ_L \tan(\beta_1 d_1)}, \tag{3}$$

$$Z_{\perp} = \frac{\eta_1}{\cos(\theta_1)}\frac{Z_L + j\eta_1 [\cos(\theta_1)]^{-1}\tan(\beta_1 d_1)}{\eta_1 [\cos(\theta_1)]^{-1} + jZ_L \tan(\beta_1 d_1)}. \tag{4}$$

ja monikerrosrakenteen impedanssia koottaessa sijoitetaan aina edellisen kerroksen impedanssi uuden kerroksen kuormaimpedanssiksi Z_L.

Käänteismuunnos on mutkattomampi, jos vielä ryhmittelemme (3):n seuraavasti:

$$\overline{\overline{Z}}_{\mathrm{eq}} = Z_{\perp}\overline{\overline{I}}_t - (Z_{\perp} - Z_{\parallel})\frac{\mathbf{k}_t\mathbf{k}_t}{k_t^2} = X\overline{\overline{I}}_t - Yk_t^2\frac{\mathbf{k}_t\mathbf{k}_t}{k_t^2}. \tag{5}$$

3 Likiarvoistus

Olettakaamme, että $k_0 d_i \ll 1$, jolloin voimme käyttää tekijää $k_t d_i$ sarjakehitelmiemme perustana, ja että

$$|k_i| d_j \leq 1. \qquad i, j \in \{1, 2, \ldots, n\}.$$

Likiarvomme pätevät parhaiten, kun aallon tulokulma ei eroa kummoisesti kohtisuorasta. Kerrosten paksuudet voivat olla kohtuullisia, jos taitekerroin ei ole kovin pieni.

Näin siis pääsemme tutkimaan kertoimien X ja Y suuruuksia, ja todettakoon lyhyesti, että induktiolla voi osoittaa monikerroksisen rakenteen kertoimien olevan suuruudeltaan seuraavia:

$$X \sim O(k_i d_j). \qquad Y \sim O(d_i / k_j). \tag{6}$$

Edellä mainittuja tietojen avulla ja muutamien laskutoimitusten jälkeen pystymme lopulta ilmoittamaan ylimmän eli n:nen kerroksen impedanssin alempien kerrosten kokonaisimpedanssin avulla [4]:

$$\overline{\overline{Z}}_{\mathrm{eq}} = X_n \overline{\overline{I}}_t + Y_n \nabla_t \nabla_t, \tag{7}$$

minkä kertoimet X_n:n ja Y_n:n voi laskea rekursiivisesti

$$X_i = \frac{X_{i-1} + j\left(\frac{X_{i-1}^2}{\eta_i} + \eta_i\right) \tan(k_i d_i) - X_{i-1} \tan^2(k_i d_i)}{\left[1 + j \frac{X_{i-1}}{\eta_i} \tan(k_i d_i)\right]^2}. \tag{8}$$

$$Y_i = \frac{Y_{i-1} + j \frac{\eta_i}{k_i^2} \tan(k_i d_i)}{\left[1 + j \frac{X_{i-1}}{\eta_i} \tan(k_i d_i)\right]^2}. \tag{9}$$

kun $i = 1 \ldots n$. Yhtälössä (7) olemme jo paluumuuntaneet Fourier-muuttujan $\mathbf{k}_t$.

Viitteet

[1] Senior T.B.A, Volakis J.: "Approximate Boundary Conditions in Electromagnetics". (IEE Press, Lontoo, 1995).

[2] Hoppe D.J. , Rahmat-Samii Y.: "Impedance Boundary Conditions in Electromagnetics". (Taylor & Francis, Washington DC., 1995).

[3] Oksanen M.I., Tretyakov S.A., Lindell I.V.: "Vector circuit theory for isotropic and chiral slabs". *J. Electromagn. Waves Applic.*, 1990. **4** pp. 613-643.

[4] Puska, P., Tretyakov, S.A., Sihvola, A.H.: "Recursive approximate boundary conditions for multilayered media", Electromagnetics Laboratory Report 267. Helsinki University of Technology. 1998.

LOW FREQUENCY ANOMALIES OF PERFECT CONDUCTORS IN A FREE SPACE

Hannu Hongisto, Geologian tutkimuskeskus, PL96, 02151 Espoo; hannu.hongisto@gsf.fi

Matti Oksama, Geologian tutkimuskeskus, PL96, 02151, Espoo; matti.oksama@gsf.fi

Introduction

Many of the economical ore bodies are highly conducting and where the overburden is thin and the hostrock is resistive, the electromagnetic responses may be modelled with a perfect conductor located in a resistive environment. In addition, the results of a perfectly conducting model can be used as reference anomalies in comparisons of other numerically more complicated solution methods.

Integral equations

In this study we have used the following integral equations, which are solved numerically by applying the point matching method with pulse functions as basis functions (Harrington, 1968). The first of these is a Fredholm integral equation of second kind for magnetic scalar potential (Furness, 1996):

$$-\frac{1}{2}\phi(\mathbf{r}) + \frac{1}{4\pi}\int_S \phi(\mathbf{r}_0)\frac{\partial}{\partial n_0}G(\mathbf{r},\mathbf{r}_0)\,ds_0 = -\phi_{prim}(\mathbf{r}), \tag{1}$$

where magnetic scalar potential ϕ and variable G are defined as follows:

$$\mathbf{H}(\mathbf{r}) = -\nabla\phi(\mathbf{r}), \qquad G(\mathbf{r},\mathbf{r}_0) = \frac{1}{|\mathbf{r}-\mathbf{r}_0|}.$$

Once the magnetic scalar potential on the surface of the body is solved, the anomalous magnetic field can be computed from the formula:

$$\mathbf{H}_{sek}(\mathbf{r}) = \frac{1}{4\pi}\nabla\int_S \phi(\mathbf{r}_0)\frac{\partial}{\partial n_0}G(\mathbf{r},\mathbf{r}_0)\,ds_0. \tag{2}$$

The second integral equation for the magnetic scalar potential (Furness, 1996) is actually a differentiated form of equation (1):

$$\frac{1}{4\pi}\int_S \phi(\mathbf{r}_0)\frac{\partial^2}{\partial n\,\partial n_0}G(\mathbf{r},\mathbf{r}_0)\,ds_0 = -\mathbf{H}_{prim}(\mathbf{r})\cdot\mathbf{n}. \tag{3}$$

The anomalous magnetic field is computed from formula (2). The integral equation (3) is valid also for a two dimensional plate, and the domain of integration is the open surface of the plate.

The third equation is a Fredholm integral equation of the second kind for magnetic surface charge (Oksama and Suppala, 1993):

$$-\frac{1}{2}S(\mathbf{r}) + \frac{1}{4\pi}\int_S S(\mathbf{r}_0)\frac{\partial}{\partial n}G(\mathbf{r},\mathbf{r}_0)\,ds_0 = \mathbf{H}_{prim}(\mathbf{r})\cdot\mathbf{n} \tag{4}$$

After solving the surface charge the anomalous magnetic field is computed as follows:

$$\mathbf{H}_{sek}(\mathbf{r}) = \frac{1}{4\pi}\nabla\int_S S(\mathbf{r}_0)G(\mathbf{r},\mathbf{r}_0)\,ds_0 \tag{5}$$

The solutions of integral equations (1) and (4) exist and are unique (Colton and Kress, 1983).

Numerical results

We have examined with four examples the numerical consistence of the three 3D integral equation solutions. The first example is a nearly equidimensional model using the AEM measuring system of the GTK. The results are computed for two flight altitudes. In this case all the solution methods yield almost equal results, in particular with the higher altitude.

In the second numerical example the electromagnetic response of a very thin plate (80 m × 80 m × 0,025 m) is calculated with all the four integral equations. A three dimensional thin body is numerically a problematic model. Three of the curves are practically the same: the equation (3) for the two dimensional plate, the equation (1) of the scalar potential, and the equation (4) of the surface charge give the curves near each other. The curve of the scalar potential equation is somewhat more accurate than the curve of the surface charge equation because it is closer to the thin sheet curve. The curve of the other scalar potential solution (3) for a three dimensional body deviates a little from the others. The accuracy of the latter scalar potential solution as well that of the surface charge solution increases clearly, when they are computed with double precision.

In the third example the convergence of electromagnetic response using integral equation (1) is studied as a function of the element density for the model of the former example. With very coarse division of 24 elements the corresponding curve oscillates strongly indicating great approximation errors.

Thereafter increasing the number of elements gradually reduces the intensity of the calculated anomaly, until with 960 elements we have the last approximation. Obviously with too low element densities this method yields too high anomaly intensities. With more equidimensional models the convergence of the anomaly intensity is much quicker when number of elements is increased.

In the last example the computed electromagnetic response by using the scalar potential solution of equation (1) is compared with the results of small scale model experiments. The small scale model is made from a bent aluminum sheet. The coil system is horisontal coplanar (slingram). In general the compared results match quite well but with the smallest distance of the coils to the body the numerical solution is most difficult.

Conclusions

Comparing the convergence rates of the results given by the different integral equations it is found that with a standard PC it is possible to get reliable anomalies even for thin plates. The integral equation (1) for potential is the most accurate, but the integral equation (4) for the surface density is almost as accurate.

References

Colton D. and Kress R. 1983. Integral equation methods in scattering theory. Pure & Applied Mathematics, John Willey & Sons.

Furness P. 1996. An integral equation for the homogeneous Neumann condition. Geophysical Prospecting, 44, 27–40.

Harrigton R.F. 1968. Field computation by moment methods. The Macmillan Publishing Co. Inc.

Ketola M. 1968. The interpretation of slingram (horizontal loop) anomalies by small-scale model measurements. Geological Survey of Finland, Espoo. Report of Investigations 1. 19 pp. + app.

Oksama M. and Suppala I. 1993. Calculation of electromagnetic anomalies of perfectly conducting bodies by integral equations. Journal of Applied Geophysics, 30, 205–213.

INTERPRETATION OF MOVING EM DIPOLE-DIPOLE MEASUREMENTS USING THIN PLATE MODELS

Matti Oksama and Ilkka Suppala
Geological Survey of Finland (GTK).
Matti.Oksama@gsf.fi
Ilkka.Suppala@gsf.fi

Introduction

The three dimensional inversion of electromagnetic data is still rather problematic, because forward modelling programs are usually time consuming. They are based on numerical methods like finite element or integral equation methods.

In this study we have chosen a specific model for interpretation: two thin plates, which are located in a horizontally layered earth with two layers. This model is rather limited, but in a few geological cases it is relevant.

We have applied this interpretation method for two geophysical EM-systems, the slingram-system and the airborne electromagnetic system of the Geological Survey of Finland (GTK).

Inversion method

Forward modelling is based on P. Weidelt's integrodifferential eguation (1979) and on the program Leroi made by Amira (1997).

We have used a measure to describe the goodness of the model:

$$\| T(\mathbf{p}) - M \| + u \| s(\mathbf{p}) \| \qquad (1)$$

where T is the theoretical data, M is the measured data, u is a scalar multiplier, $\mathbf{p}$ is a parameter vector and s is a function of $\mathbf{p}$. The norms are L2-norms. The first term measures the goodness of fit and the second, depending on the function s, gives a possibility for regularization, weighting and constraining of the model parameters.

To minimize the measure we have applied the trust region Levenberg-Marquardt optimization method. We have used the programs ODRPACK (Boggs et al, 1989) and TENSOLVE (Bouaricha and Schnabel, 1997). Our simulations showed that ODRPACK requires a lower (or equal) number of forward calculations.

Numerical examples

First the inversion routine has been tested by calculating the theoretical anomalies and interpreting them. The slingram (HLEM) and AEM-system of GTK was used. The time of inversion depends on the number of forward calculations. Jacobian matrices are calculated using finite differences of the numerically evaluated function, which means at least $m+1$ calculations for every iteration, where m is the number of parameters to be estimated.

The forward parametric model is a function of the number of elements. If the number of elements can change automatically (depending on the size of the plate) during iterations, this can cause local minima. Too coarse discretization in forward calculations changes the theoretical data. The coarser the discretization, the more the minimum point moves in the parameter space.

Example 1

We have studied the effect of measurement errors on the interpretation errors in the AEM-system of GTK by Monte Carlo simulations. The examined model is composed of two layers and a plate. Typical errors are due to noise and changes in levelling. The statistics of the added errors are the following: the standard deviation (STD) of the noise is 5 ppm in the in-phase data, 10 ppm in the quadrature data, the STD of levelling errors is 10 ppm for the in-phase data and 15 ppm for the quadrature data, Fig 1 a. The estimated parameters are resistivity of the first layer ρ_1, thickness h_1, depth, profile coordinate, dip and conductivity-thickness product of the plate σt.

The data is first interpreted using TENSOLVE with only the L2-norm of the difference between theoretical and measured data, Fig 1 b. It is also interpreted using regularization and by constraining the resistivity of the first layer ρ_1 to the range 350–400 Ωm with the same program, Fig 1 c. Without regularization and constraining, the parameters of the first layer show large variation, but with a priori information the variation is reduced. The dip angle in particular is rather sensitive to errors.

The minimized sum of squares as a function of the dip angle and the profile coordinate (distance) of the plate shows the global and a local minimum of the measure. The local minimum may be caused by the correlation between the dip angle and the distance. The plate model with the deepest dip angle (Fig. 1 c) is associated with this local minimum. Also the known correlation between the conductivity and the thickness of the first layer is clearly seen in the coordinate system defined by these parameters.

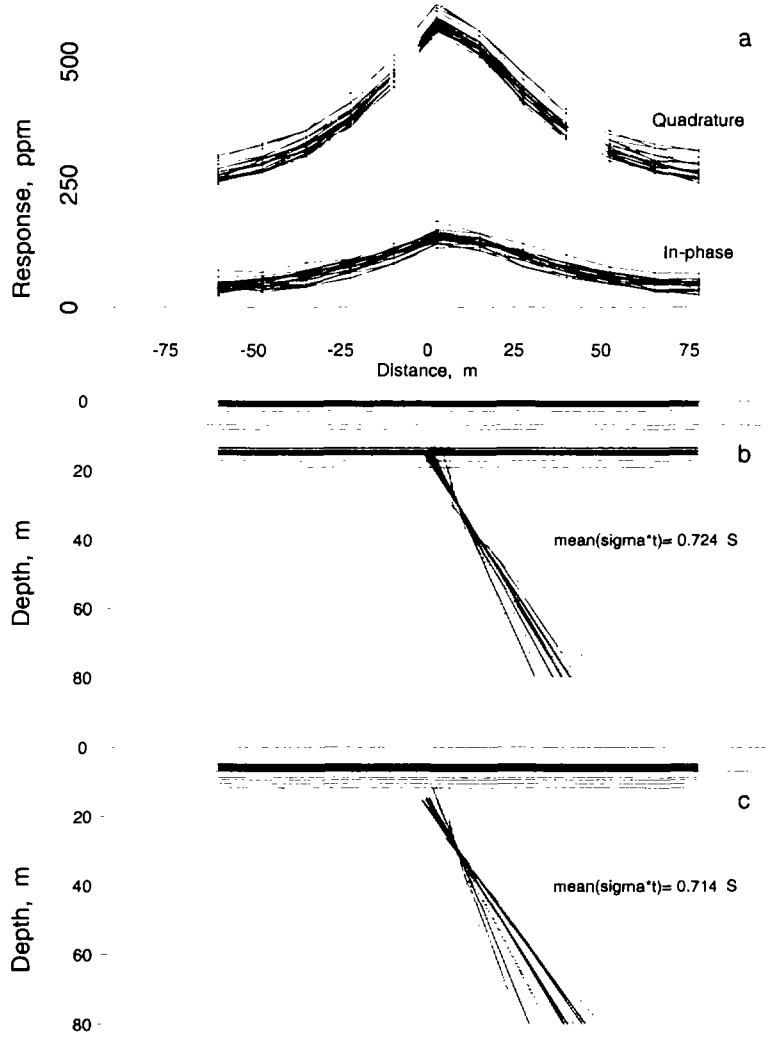

Figure 1. *Effect of simulated measurement errors on the interpretation parameters, a) the data sets, b) and c) interpretations (sigma*t means σt).*

Example 2

Fig. 2 shows the interpretation results of the small scale measurements of two plates. They are made with the slingram system by Ketola (1968). The experimental model curves are digitized and the interpolated data are interpreted. The interpretation prodecure gives the model parameters close to those applied by Ketola. The scaled values for the small scale parameters are: the coil separation is 60 m, the frequency is 3600 Hz, the plates are at 6 m depth, the separation of the plates is 30 m, the sizes of the plates are 300×300 m^2 and the conductivity-thickness products are 1.02 S.

The estimated sizes are: the average strike lengths are 173 m and 243 m for the left and the right plate, and the conductivity-thickness products are 1.28 S and 1.13 S, respectively. The strike length 173 m is not effectively quite infinite and that's why this plate is estimated to be more conductive. The values of estimated parameters, dip angle especially, depend slightly on the interpolation of the points, data sets 1,2 and 3 in Fig 3.

We have also interpeted this data with one plate model, and then the theoretical and measured curves are clearly different. The difference between one and two plate data was distinct also for the deeper situated plates (18 m).

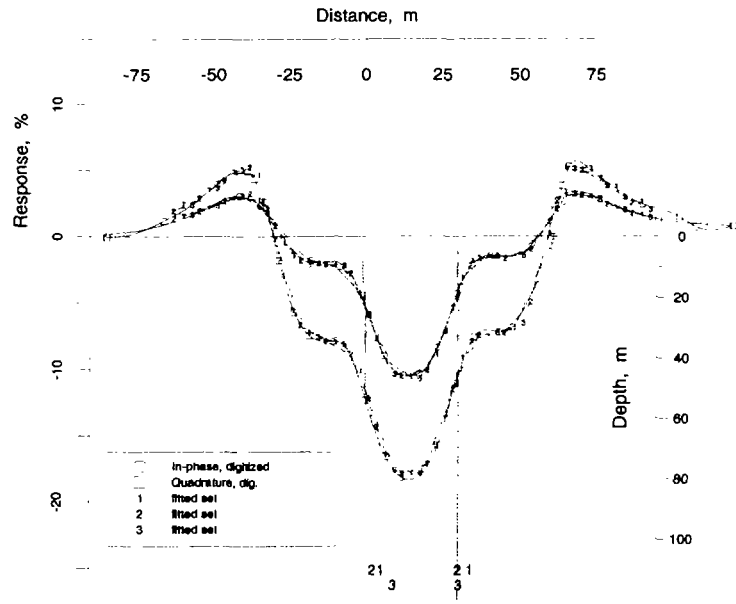

Figure 2. *Digitized small scale experiments of Ketola and the results of interpretation.*

References

Amira, 1997, Mathematical geophysics group CRC for Australian mineral exploration technologies.

Bouaricha, A., and Schnabel, R.,B., 1997, Algorithm 768: TENSOLVE: A software package for solving systems of nonlinear equations and nonlinear least-squares problems using tensor methods: ACM Trans. Math. Software, **23**(2), 174–195.

Boggs, P.T., Donaldson, J.R., Byrd, R.H., and Schnabel, R.B., 1989, Algorithm 676—ODRPACK: Software for weighted orthogonal distance regression: ACM Trans. Math. Software, **15**(4), 348–364.

Ketola, M., 1968, The interpretation of slingram (horizontal loop) anomalies by small-scale model measurements: Geological Survey of Finland, Report of Investications 2. 35 pp.+app.

Weidelt, P., 1979, Researcher course in Oulu, Finland.

MODELLING OF THREE COMPONENT EM BOREHOLE RESPONSE

Heikki Soininen, Risto Mononen and Matti Oksama*
Geological Survey of Finland
PO.Box 96
FIN-02151 ESPOO
Finland

This paper presents numerical modelling results for EM borehole-system, in which both the axial magnetic dipole transmitter and the three component receiver are in the same borehole. Calculations are carried out with the software based on volume integral equation formulation (MARCO code).

The accuracy of the software was tested by comparing numerical calculation results against physical scale model results. Scale modelling was performed by VIRG-Rudgeofika, St. Petersburg. The model used in comparison was a 100 m × 100 m × 25 m rectancular block with resistivity of 1 Ωm and 5 Ωm (full scale). Resistivity contrasts between the half-space and the model were 70, 500 and 800. Frequencies from 2100 Hz to 10000 Hz and 4750 Hz were used and the transmitter-receiver distance (coil separation) was 60 and 90 m. Lead, aluminium and copper were used as a model material. The model was embedded in graphite. Six measuring holes were bored in graphite and in metal.

The comparison between calculated and measured profiles demonstrates that the volume integral equation solution deteriorates as the contrast increases. The solution may be unreliable when the contrast exceeds 500, especially when the hole pass through the conductive block.

The behaviour of the response of the borehole EM system was studied using a rectangular body as a model, both passed and intersected by the drillhole. The resistivity of the body was 5 Ωm and that of the environment 500 Ωm (resistivity contrast 100). Coil separation was varied from 30 m to 120 m.

With the parameters used in this study it is possible to detect a target at a distance exeeding 100 m. The use of several coil separations in the same hole improves the capabilities for interpretation of model parameters.

The axial component reveals the position of the conductor along the drillhole. The distance to the body can be roughly classified using measuring data into groups *far away*, *near* and *intersection*.

As the signs of the radial components depend on the quarter of the space containing the conductor, they can be used to determine the direction to the conductor.

This work was supported by the European Commission in the framework of Brite Euram programme (BE-117).

FI9800124

STUK-A156

ELECTROMAGNETIC PROBLEMS IN NUCLEAR WASTE DISPOSAL

Esko H. Eloranta
Radiation and Nuclear Safety Authority (STUK)
P.O. Box 14, FIN-00881 Helsinki, FINLAND
esko.eloranta@stuk.fi

Electromagnetism is needed when final disposal of nuclear waste is planned and carried out. The present disposal plans include the encapsulation of spent nuclear fuel in copper-steel canisters the height of which is about 4.5 m and diameter about 1 m. These canisters (nearly 2000 canisters in total) will be put in holes at the bottom of deposition tunnels to be excavated at a depth of about 500 m in crystalline bedrock. There are especially two areas in which electromagnetism plays an important role. These are (1) electromagnetic characterization of fractured rock before any constructions are made and during the construction of the repository, and (2) electromagnetic safeguards monitoring of a repository.

1 Electromagnetic characterization of fractured rock

The crystalline bedrock is characterized by fractures on different geometrical scales. One of the basic problems is to acquire data about the fracturing because fractures control groundwater flow and radionuclide migration, which are the central issues in the safety analyses of disposal. Fractured rock behaves anisotropically when it is studied electromagnetically by DC and AC methods. Especially electrical conductivity anisotropy is an important property. Thus, the anisotropic structural models are relevant in the study of fractured rock mass. STUK has had a research project in collaboration with the Electromagnetics Laboratory of the Helsinki University of Technology from 1991 onwards in the calculation of electromagnetic fields of anisotropic models. The project has been described in [1]. Many basic problems were treated by image theory. These geometries included a half-space bounded by a *perfect electric conductor,* by *a perfect magnetic conductor,* and by *an impedance boundary.* Furthermore an anisotropic *layer* model was studied and finally, after various sequential relaxations, a *very general anisotropic half-space prob-*

lem could be solved by Heaviside operational calculus. Also an anisotropic, *inhomogeneous medium* could be handled with *integral equations*. A *wedge* geometry was treated as an extension to the traditionally used two parallel plate model of a fracture. The transformation of fracturing to anisotropy is also an important area of research. This is done by using so called *electromagnetic mixing formulas or rules* originally developed for microwave technology.

During various phases of disposal investigations we have varying possibilities to be in contact with fractured rock mass. In the preliminary investigation phase when only surface or bore hole measurements can be made, the half-space with air-Earth boundary forms one of the basic geometries. This corresponds to the perfect magnetically conducting boundary. When shafts and tunnels are constructed we can make measurements on the surfaces of the shafts and tunnels within the Earth. Because of excavation, there forms a so called *excavation disturbed zone (EDZ)* around the shafts and tunnels. Depending on the scale, this zone corresponds electrically to an impedance layer the conductivity of which differs from that of beneath it. The zone is also fractured and therefore anisotropic in character.

The vicinity of a deposition hole should be carefully studied in terms of fracturing before it can be accepted to host a copper-steel canister containing spent fuel. It is probable that some sort of electromagnetic systems will be used in this context to infer the fracturing.

2 Electromagnetic safeguards monitoring

The purpose of safeguards monitoring is to reveal and prevent unauthorized transfer of nuclear material from the repository to nuclear explosives or to other unknown purposes. Safeguards related to a geological repository can concern either an open repository or a closed repository. In the use of an open repository, the verification of the presence of copper-steel canisters is more or less a straightforward task where different geophysical methods can be utilized, e.g. electrical, inductive and radar methods. On the other hand, the verification of copper-steel canisters in a closed repository is a much more difficult problem.

It has been suggested that electromagnetic methods could be used also in the case of a closed repository. Requirements for the reliability and resolution capabilities of the monitoring systems are strong. The Finnish disposal plans, however, rest on the principle that no active monitoring is needed after the closure of the repository.

The main preconditions to study the potential use of geoelectromagnetic methods for monitoring purposes lie in the following facts. (1) The electrical conductivity of copper is very high (ca. 10^8 S/m), (2) the electrical conductivity of the surrounding granite-type rock mass on the other hand is very low as compared to that of the copper (ca. 10^{-7} to 10^{-3} S/m) depending, however, mainly on the water-content, i.e. fracturing and porosity of the rock mass, and the temperature, (3) the great variety of geoelectromagnetic methods as regards sources, measuring frequencies (from pure DC to radio waves), measuring configurations, and the use of time domain and frequency domain, and (4) advanced mathematical modelling techniques and procedures for electromagnetic fields and for their inversion.

Finland has made a proposal to the international safeguards community to study the potential of electromagnetic methods for closed repositories [2].

References

[1] Eloranta, E., Ermutlu, M., Flykt, M., Lindell, I., Nikoskinen, K. and Sihvola, A., 1998. *Electromagnetic characterization of fractured rock for geological disposal studies of spent nuclear fuel.* Radiation and Nuclear Safety Authority, Report STUK-YTO-TR 145, April 1998.

[2] Eloranta, E.H., Ruokola, E. and Tarvainen, M., 1997. *Post-closure monitoring of a spent fuel repository using geophysical techniques.* IAEA Symposium on International Safeguards, 13–17 October 1997, Vienna, Austria, Extended Synopses, IAEA-SM-351, p. 21.

STUK-A reports

STUK-A155 Salomaa S, Eloranta E, Heimbürger H, Järvinen H, Jokela K (toim.). Säteilyturvakeskuksen tutkimushankkeet 1998 – 2000. Helsinki 1998.

STUK-A154 Puhakainen M, Suomela M. Detection from radionuclides originating from nuclear power plant in sewage sludge. Helsinki 1998.

STUK-A153 Toivonen H, Honkamaa T, Ilander T, Leppänen A, Nikkinen M, Pöllänen R, Ylätalo S. Automated high-volume aerosol sampling station for environmental radiation monitoring. Helsinki 1998.

STUK-A152 Servomaa A (toim.). Säteilyturvallisuus ja laadunvarmistus röntgendiagnostiikassa 1998. Helsinki 1998.

STUK-A151 Voutilainen A, Mäkeläinen I, Pennanen M, Reisbacka H, Castrén O. Radonatlas över Finland. Helsinki 1998.

STUK-A150 Voutilainen A, Mäkeläinen I, Reisbacka H, Castrén O. Radonhalten i finländska bostäder. Helsinki 1998.

STUK-A149 Toivonen H, Ikäheimonen TK, Leppänen A, Pöllänen R, Rantavaara A, Saxén R, Likonen J, Zilliacus R. Application of various laboratory assay techniques to the verification of the comprehensive nuclear test ban treaty. Analyses of samples from Kuwait and from Aftac. Helsinki 1997.

STUK-A148 Voutilainen A, Mäkeläinen I, Pennanen M, Reisbacka H, Castrén O. Suomen radonkartasto. Helsinki 1997.

STUK-A147 Karppinen J. Röntgentutkimushuoneen säteilysuojauksen laskeminen. Helsinki 1997.

STUK-A146 Voutilainen A, Mäkeläinen I, Reisbacka H, Castrén O. Asuntojen radonpitoisuus Suomessa. Helsinki 1997.

STUK-A145 Ilus E (ed.). Dating of sediments and determination of sedimentation rate. Proceedings of a seminar held in Helsinki 2-3 April 1997. Helsinki 1998.

STUK-A144 Rannikko S, Karila KTK, Toivonen M. Patient and population doses of X-ray diagnostics in Finland. Helsinki 1997.

STUK-A143 Helariutta K, Rantavaara A, Lehtovaara J. Turvesoiden ja polttoturpeen radionuklidit. Helsinki 1997.

STUK-A142 Auvinen A. Cancer risk from low doses of ionizing radiation. Helsinki 1997.

STUK-A141 Jokela K, Leszczynski D, Paile W, Salomaa S, Puranen L, Hyysalo P. Matkapuhelimien ja tukiasemien säteilyturvallisuus. Helsinki 1997.

STUK-A140 Moring M, Markkula M-L. Cleanup techniques for Finnish urban environments and external doses from 137Cs - modelling and calculations. Helsinki 1997.

STUK-A139 Tapiovaara M, Lakkisto M, Servomaa A. PCXMC. A PC-based Monte Carlo program for calculating patient doses in medical x-ray examinations. Helsinki 1997.

STUK-A138 Lindell B Boice JD, Sinnaeve J, Rytömaa T. Past and future trends of radiation research. Proceedings of the seminar at STUK in Helsinki 28 February 1997. Helsinki 1997.

STUK-A137 Arvela H, Ravea T. Radonturvallinen rakentaminen Suomessa. Helsinki 1997.

STUK-A136 Pennanen M., Mäkeläinen I. & Voutilainen A. Huoneilman radonmittaukset Kymen läänissä: Tilannekatsaus ja radonennuste. Helsinki 1996.

STUK-A135 Hyvärinen J. On the fundamentals of nuclear reactor safety assessments. Inherent threads and their implications. Helsinki 1996.

STUK-A134 Ylätalo S, Karvonen J, Ilander T, Honkamaa T, Toivonen H. Doserate mapping and search of radioactive sources in Estonia. Helsinki 1996.

STUK-A133 Rantavaara A. Puutavaran radioaktiivisuus. Helsinki 1996.

STUK-A132 French S, Finck R, Hämäläinen RP, Naadland E, Roed J, Salo A, Sinkko K. Nordic Decision Conference: An exercise on clean-up actions in an urban environment after a nuclear accident. Helsinki 1996.

STUK-A131 Mustonen R, Koponen H. Säteilyturvakeskuksen tutkimushankkeet 1996 - 1997. Helsinki 1996.

STUK-A130 Honkamaa T, Toivonen H, Nikkinen M. Monitoring of airborne contamination using mobile units. Helsinki 1996.

STUK-A129 Saxén R, Koskelainen U. Radioactivity of surface water and fresh water fish in Finland in 1991-1994. Helsinki 1995.

STUK-A128 Savolainen S, Kairemo K, Liewendahl K, Rannikko S. Radioimmunoterapia. Hoidon radionuklidit ja annoslaskenta. Helsinki 1995.

STUK-A127 Arvela H. Asuntojen radonkorjauksen menetelmät. Helsinki 1995.

STUK-A126 Pöllänen R, Toivonen H, Lahtinen J, Ilander T. OTUS-reactor inventory management system based on ORIGEN 2. Helsinki 1995.

STUK-A125 Pöllänen R, Toivonen H, Lahtinen J, Ilander T. Transport of large particles released in a nuclear accident. Helsinki 1995.

STUK-A124 Arvela H. Residential radon in Finland: Sources, variation, modelling and dose comparisons. Helsinki 1995.

STUK-A123 Aaltonen H, Laaksonen J, Lahtinen J, Mustonen R, Rantavaara A, Reponen H, Rytömaa T, Suomela M, Toivonen H, Varjoranta T. Ydinuhkat ja varautuminen. Helsinki 1995.

STUK-A122 Rantavaara A, Saxén R, Puhakainen M, Hatva T, Ahosilta P, Tenhunen J. Radioaktiivisen laskeuman vaikutukset vesihuoltoon. Helsinki 1995.

STUK-A121 Ikäheimonen TK, Klemola S, Ilus E, Sjöblom K-L. Monitoring of radionuclides in the vicinities of Finnish nuclear power plants in 1991-1992. Helsinki 1995.

STUK-A120 Puranen L, Jokela K, Hietanen M. Altistumismittaukset suurtaajuuskuumentimien hajasäteilykentässä. Helsinki 1995.

STUK-A119 Voutilainen A, Mäkeläinen I. Huoneilman radonmittaukset Itä-Uudenmaan alueella: Tilannekatsaus ja radonennuste. Askola, Lapinjärvi, Liljendal, Loviisa, Myrskylä, Mäntsälä, Pernaja, Pornainen, Porvoo, Porvoon mlk, Pukkila, Ruotsinpyhtää ja Sipoo. Helsinki 1995.

STUK-A118 Reiman L. Expert judgment in analysis of human and organizational behaviour in nuclear power plants. Helsinki 1994.

STUK-A117 Auvinen A, Castrén O, Hyvönen H, Komppa T, Mustonen R, Paile W, Rytömaa T, Salomaa S, Servomaa A, Servomaa K, Suomela M. Säteilyn lähteet ja vaikutukset. Helsinki 1994.

The full list of publications is available from

STUK—Radiation and Nuclear Safety Authority
P.O. BOX 14
FIN-00881 HELSINKI, Finland
Tel. +358 9 759 881

STUK

STUK-A156 The eighth National Electromagnetics Meeting on August 27, 1998

ISBN 951-712-267-5
ISSN 0781-1705

Oy Edita Ab, Helsinki 1998